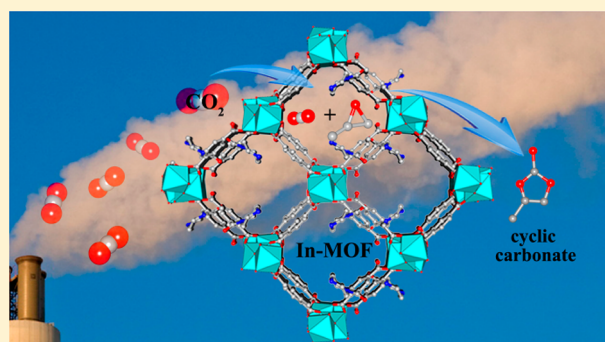


Exceptionally Robust In-Based Metal–Organic Framework for Highly Efficient Carbon Dioxide Capture and Conversion

Lin Liu,[†] Shi-Ming Wang,[†] Zheng-Bo Han,^{*,†} Meili Ding,[‡] Da-Qiang Yuan,[§] and Hai-Long Jiang^{*,‡,§}[†]College of Chemistry, Liaoning University, Shenyang 110036, P. R. China[‡]Hefei National Laboratory for Physical Sciences at the Microscale, Collaborative Innovation Center of Suzhou Nano Science and Technology, Department of Chemistry, University of Science and Technology of China, Hefei, Anhui 230026, P. R. China[§]State Key Laboratory of Structural Chemistry, Fujian Institute of Research on the Structure of Matter, Chinese Academy of Sciences, Fuzhou 350002, P. R. China

Supporting Information

ABSTRACT: An In-based metal–organic framework, with 1D nanotubular open channels, $\text{In}_2(\text{OH})(\text{btc})(\text{Hbtc})_{0.4}(\text{L})_{0.6} \cdot 3\text{H}_2\text{O}$ (1), has been synthesized via an in situ ligand reaction, in which 1,2,4- H_3btc is partially transformed into the L ligand. Compound 1 exhibits exceptional thermal and chemical stability, especially in water or acidic media. The activated 1 presents highly selective sorption of carbon dioxide (CO_2) over dinitrogen. Interestingly, diffuse-reflectance infrared Fourier transform spectroscopy with a carbon monoxide probe molecule demonstrates that both Lewis and Brønsted acid sites are involved in compound 1. As a result, as a heterogeneous Lewis and Brønsted acid bifunctional catalyst, 1 possesses excellent activity and recyclability for chemical fixation of CO_2 coupling with epoxides into cyclic carbonates under mild conditions. In addition, the mechanism for the CO_2 cycloaddition reaction has also been discussed.



1. INTRODUCTION

Anthropogenic-emitted carbon dioxide (CO_2) is the main greenhouse gas causing the greatest environmental concerns.¹ The emissions mainly originate from the combustion of the coal, oil, and natural gas.² Nowadays, more and more protocols have been proposed to solve the problem.³ The fundamental way is to explore clean energy; however, large-scale industrial implementation is not sufficient to change the energy consumption structures in a short time. Thus, carbon capture and sequestration (CCS) technologies would be an efficient way to capture CO_2 from existing emission sources.⁴

The state-of-art technology of CCS technologies, the amine-based wet scrubbing approach, is widely accepted.⁵ However, it still suffers from high cost by regeneration, equipment corrosion, and solvent boiloff. As a renewable C1 feedstock, CO_2 can be utilized as an economic, nontoxic, and renewable reactant.⁶ However, because of the thermodynamic and kinetic stability of CO_2 , the chemical fixation of CO_2 is not easy. Therefore, it is imperative and attractive to develop methods to activate and convert CO_2 catalytically to high-value chemicals. Particularly, the coupling of CO_2 with epoxides into cyclic carbonates is a very efficient route for CO_2 utilization.⁷ The cyclic carbonates are a kind of chemical intermediate in the production of plastics, organic solvents, and so on.⁸ Homogeneous and heterogeneous catalysts have been developed for the cycloaddition of CO_2 and epoxides. To date, considerable homogeneous catalysts, including quaternary

ammonium and phosphonium salts,⁹ ionic liquids,¹⁰ alkali-metal salts,¹¹ Schiff bases,¹² and metal-centered salen complex,¹³ have been employed to promote transformation. Although they show effective conversion of the coupling of CO_2 with epoxides into cyclic carbonates, the inherent shortcomings of separation of the product and recycling of the catalyst limit the wide application of the homogeneous catalysts. Consequently, in order to overcome the defect of the homogeneous catalyst, heterogeneous catalysts, such as metal oxides,¹⁴ functional polymers,¹⁵ and zeolites,¹⁶ have been developed. However, most of them need high temperature ($>100\text{ }^\circ\text{C}$) to activate the reaction, which increases the cost of the reaction process. There are several requirements for an efficient heterogeneous catalyst for the cycloaddition of CO_2 and epoxide: first, high surface area and CO_2 adsorption capacity; second, enough Lewis/Brønsted acidic or basic sites to activate the epoxide/ CO_2 ; third, high stability and long durability upon exposure to the reaction conditions.

Metal–organic frameworks (MOFs) are a class of crystalline porous organic–inorganic hybrid materials by the combination of metal centers or clusters and organic ligands, which may be the most promising candidates to satisfy the dual challenge of CO_2 capture and conversion.¹⁷ They possess large surface area and well-ordered porous structure and, most importantly, could

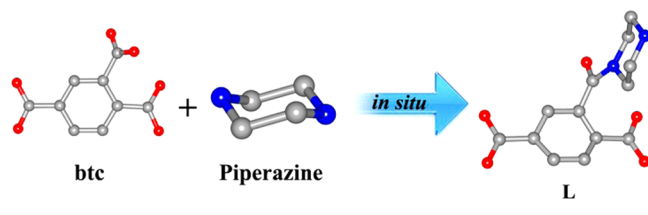
Received: January 10, 2016

Published: March 14, 2016

be designed to selectively capture CO₂.¹⁸ Many strategies are employed to reinforce the CO₂ capture ability of MOFs. For example, the creation of unsaturated metal sites and decoration of the pores with basic molecules at the open metal sites and the basic pore surface could result in effective enhancement of the CO₂ adsorption.¹⁹ In addition, MOFs are employed as types of heterogeneous catalysts in the past decades that usually contain Lewis acidic sites, Brønsted acidic sites, Lewis basic sites, and other catalytically active sites.²⁰ For example, Cu₃(BTC)₂,²¹ ZIF-8,²² Cr-MIL-101,²³ MOF-5,²⁴ UIO-66,²⁵ MMFC-2,²⁶ and USTC-253²⁷ have been reported for the synthesis of cyclic carbonates from CO₂ and epoxides. Therefore, the strategies to realize the high CO₂ uptake and high activity for CO₂ conversion are coincident, which is attractive for reducing CO₂ emissions, while there are only a few MOFs that can meet the two requirements of exhibiting high adsorption capacity of CO₂ and having enough Lewis or Brønsted acidic sites at the same time. In addition, chemical and thermal stability is a precondition of the heterogeneous catalyst in practical applications. Therefore, it is imperative to design new MOFs with catalytic centers, high CO₂ adsorption, and high stability based on the devisible nature of MOFs.

In this study, an exceptionally robust MOF compound, In₂(OH)(btc)(Hbtc)_{0.4}(L)_{0.6}·3H₂O (**1**), which features a 3D porous architecture with 1D nanotubular open channels, has been synthesized via in situ ligand reaction (Scheme 1). The

Scheme 1. Illustration of in Situ Formation of the L Ligand



high adsorption capacity of CO₂ and high-density open catalytic sites in the pores make it a highly efficient Lewis/Brønsted acid bifunctional heterogeneous catalyst for CO₂ coupling with epoxides into cyclic carbonates under mild conditions. In addition, the reusability and truly heterogeneous nature of the catalyst for the reaction has also been demonstrated.

2. EXPERIMENTAL SECTION

2.1. Materials and Methods. All starting materials employed were commercially available and were used without further purification. The Fourier transform infrared (FT-IR) spectra were recorded from KBr pellets in the 4000–500 cm⁻¹ range on a Nicolet SDX spectrometer. Thermogravimetric analysis (TGA) was performed on a PerkinElmer Pyris 1 [25–700 °C, 5 °C min⁻¹, flowing N₂(g)]. Powder X-ray diffraction (PXRD) was recorded with a Bruker AXS D8 advanced automated diffractometer with Cu K α radiation. Variable-temperature PXRD studies were heated at a constant rate of 5 °C min⁻¹ from room temperature to 50, 100, 150, 200, 250, 300, and 350 °C in air, respectively. The C, H, and N microanalyses were carried out with a PerkinElmer 240 elemental analyzer. Solid-state NMR spectra were collected on a Bruker AVANCE III 600 spectrometer. ¹H NMR spectra were recorded on a Varian-300 MHz NMR spectrometer. The dinitrogen (N₂) adsorption isotherm was measured at 77 K using a liquid-N₂ bath. The CO₂ adsorption isotherm was measured at 273 K using an ice/water bath and at 298 K using a water bath. The diffuse-reflectance infrared Fourier transform (DRIFT) spectroscopy of carbon monoxide (CO) adsorption was obtained on a Nicolet iS10

spectrometer with a mercury–cadmium–telluride (MCT) detector and a low-temperature reaction chamber (Praying Mantis Harrick). The sample was activated completely before DRIFT characterization. Then, an appropriate amount of sample powder was loaded into the IR reflectance cell and purged by flowing helium (20 mL min⁻¹) for 120 min at 423 K under vacuum to remove the adsorbed water, and then the cell was cooled to 173 K with liquid N₂. CO adsorption was carried out by generally introducing 10% CO/He (5 mL min⁻¹) to the IR reflectance cell for almost 20 min. The product yield of the catalysis reaction was monitored by an Agilent 7890A gas chromatograph equipped with a HP-5 column (30 m \times 320 μ m \times 0.25 μ m; injector temperature 250 °C) and a hydrogen flame ionization detector. N₂ and CO₂ adsorption–desorption experiments were carried out on an automated gas sorption analyzer (Quantachrome Instruments ASiQ-C).

2.2. Synthesis of In₂(OH)(btc)(Hbtc)_{0.4}(L)_{0.6}·3H₂O (1**).** The synthetic method of **1** was modified according to the previously reported literature by our group.²⁸ In(NO₃)₃·4.5H₂O (50 mg), 1,2,4-H₃btc (80 mg), and 100 mg of piperazine in 3 mL of water were mixed in a 10 mL Teflon reactor. The mixture was heated in a 160 °C oven for 72 h. After cooling to room temperature, light-yellow rodlike crystals were harvested by filtration, washed with water, and dried in air (73 mg, 72% yield). Anal. Calcd for **1**: C, 32.38; H, 2.50; N, 2.22. Found: C, 32.60; H, 2.84; N, 2.01. FT-IR (KBr, cm⁻¹): 3431 (m), 2924 (w), 1622 (vs), 1582 (vs), 1489 (s), 1385 (vs), 1302 (m), 1285 (m), 1254 (w), 1170 (m), 1077 (m), 1044 (w), 1023 (w), 1007 (w), 915 (m), 815 (s), 720 (s), 705(w), 666 (m), 542 (s).

2.3. X-ray Crystallography. Crystallographic data of the complex were collected at 100 K with an Apex II diffractometer with Mo K α radiation (λ = 0.71073 Å) and a graphite monochromator using the ω -scan mode. The structure was solved by direct methods and refined on F² by full-matrix least squares using the SHELXTL-2014 crystallographic software package.²⁹ Two guest water molecules were highly disordered, and attempts to locate and refine the peaks were unsuccessful. The diffused electron densities resulting from these residual molecules were removed from the data set using the SQUEEZE³⁰ routine of PLATON and refined further using the data generated. The contents of guest water molecules are not represented in the unit cell contents for the crystal data. Crystallographic data for structural analyses are summarized in Table S1. The CCDC reference number is 1437309 for **1**.

2.4. Catalytic Performance Evaluation. Before the reaction, the catalyst was activated at 423 K for 12 h under vacuum to remove the guest water molecule. The catalytic reactions at high pressure were carried out in a 25 mL stainless steel high-pressure reactor. The activated catalyst was transferred to the reactor immediately. The temperature of the reactor was increased and maintained at 80 °C, and the reactor was pressurized with CO₂ up to 2.0 MPa. The reaction mixture was stirred (500 rpm) under pressurized conditions for 4 h and catalyzed by activated **1** and a cocatalyst of tetra-*n*-tert-butylammonium bromide (TBAB). When the reaction was completed, the reactor was quickly cooled in cold water. The catalytic reactions at ambient temperature and pressure were carried out in a 10 mL Schlenk tube using epoxide (20 mmol) with CO₂ catalyzed by activated **1** and a cocatalyst of TBAB for 48 h. The products were monitored by gas chromatography–mass spectrometry (GC–MS). After catalytic reactions, the catalyst was separated by centrifugation and the product yields were determined by GC. The catalyst was isolated from the reaction solution at the end of the catalytic reaction, washed with ethanol three times, dried at 423 K for 12 h under vacuum, and then reused in the second run of the reaction.

3. RESULTS AND DISCUSSION

3.1. Crystal Structure. The synthetic method of **1** was modified according to the previously reported literature.²⁸ We recollected the crystal data of **1**, which revealed that part of 1,2,4-H₃btc reacted with piperazine to form the L ligand. After carefully comparing the structure of **1** with the previously reported structure, we found that they were almost the same.

The previous data were not good, and therefore the partial occupancy of piperazine was not solved. In this work, with high-quality single crystals and other characterization tools, we were able to decide on the exact structure. Herein, we redescribe the crystal structure of **1**. It features a 3D porous network with 1D nanotubular open channels. The asymmetric unit consists of two In^{III} centers, one μ_2 -OH group, one btc ligand, 0.4 Hbtc, 0.6 L ligand, and one lattice water molecule, in which the L ligand is derived from 1,2,4-H₃btc and piperazine via an in situ ligand reaction (Figure S1). The C13, C14, C15, C16, and C18 atoms of the Hbtc and L ligands are disordered. The ratio between the Hbtc and L ligands was decided by elemental analysis and ¹H NMR integral results. The binuclear In^{III} subunits are connected through μ_2 -OH groups to form an extended zigzag {In–OH–In}_n chain along the *b* axis (Figure S2). Furthermore, the four extended infinite chains were connected by the btc and L or Hbtc ligands to form a 1D nanotubular open channel that runs through the crystallographic *b* axis with a cross section of approximately 16.3 × 15.5 Å² (Figure 1a,b). The only channel is further connected by the

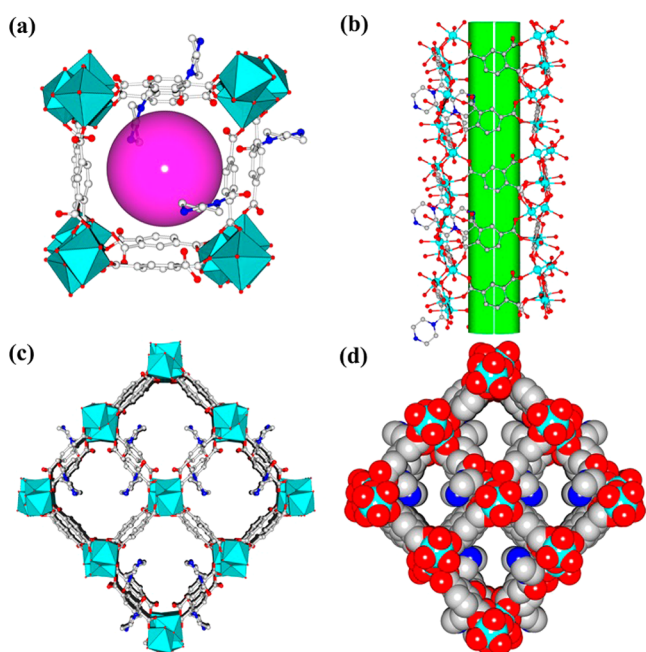


Figure 1. (a) Polyhedral presentation of the 1D channel of **1**. (b) Ball-and-stick representation of the 1D channel along the *b* axis. (c) 3D single network of **1**. (d) Space-filling representation of **1** along the *b* axis. Color code: In, turquoise; C, gray; N, blue; O, red.

btc and L ligands to give rise to a 3D porous structure (Figure 1c,d). In addition, the total accessible volume of the unit cell was estimated to be 2346.6 Å³ using PLATON,³¹ which accommodates lattice solvent molecules and is approximately 34.6% of the unit-cell volume (6775.1 Å³). In order to confirm the in situ formed L ligand, ¹³C CPMAS NMR spectroscopy of the as-synthesized **1** and H₃btc ligand was performed. As shown in Figure S3, the chemical shifts around 170 ppm are ascribed to the carboxylate C atoms and the chemical shifts around 135 ppm are ascribed to the aromatic C atoms. In contrast to the ¹³C CPMAS NMR spectra of 1,2,4-H₃btc, the new chemical shifts around 45 ppm for **1** are ascribed to the C atoms of piperazine. Compared with 1,2,4-H₃btc, two new peaks at δ 3.1 and 3.3 of the ¹H NMR spectrum of **1** (Figure S4) were

assigned to the hydrogen signals of piperazine, which further verified that part of 1,2,4-H₃btc reacted with piperazine to form the L ligand. Furthermore, the ratio between the Hbtc and L ligands is confirmed by the ¹H NMR integral results.

3.2. Thermal and Chemical Stability. The phase purity of **1** was verified by PXRD studies. The diffraction pattern of **1** was consistent with the calculated pattern, which indicated the high phase purity of the freshly prepared **1** (Figure S5). PXRD at varying temperatures in air was also carried out to investigate the thermal stability of **1**. As shown in Figure S6, the experimental diffraction patterns of **1** were all consistent with the calculated ones from ambient temperature to 300 °C with a temperature increase gradient of 50 °C. The diffraction pattern had no obvious change until the temperature increased to 350 °C, where the peaks at 12, 13, and 16° disappeared, which indicated that **1** remained stable until the environmental temperature exceeded 300 °C. The high thermal stability of **1** also made it possible to use it in broad temperature ranges. The chemical stability of **1** was tested by refluxing **1** in boiling organic solvents [hexane, propylene carbonate (PC), dimethyl sulfoxide, alcohol], water, and even a 0.01 M HCl solution for 24 h (Figure 2). The unaltered PXRD patterns indicated that

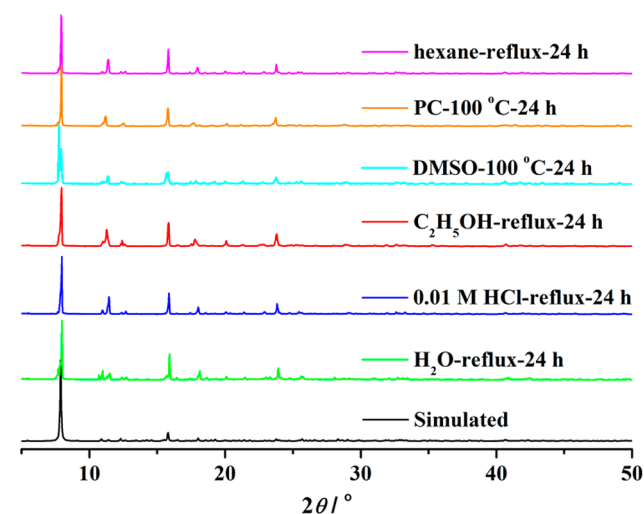


Figure 2. Chemical stability tests for **1** monitored by PXRD analysis.

the crystallinity of **1** was well retained after solvent treatment. It is reported that the greater basicity of the pore would benefit from increasing the stability of the framework and the azolate-based MOFs usually exhibit excellent stability.³² It can be concluded that the robustness of **1** could be attributed to the coordinated piperazine, which increases the basicity of the pores. This kind of exceptional thermally and chemically stable MOF is quite rare among the reported MOFs.³³ TGA curves of **1** and activated **1** are shown in Figure S7, which indicates that the weight loss in the temperature range from 25 to 150 °C corresponds to the loss of guest water molecules. The difference between the as-synthesized **1** and activated **1** could be ascribed to the removal of a guest water molecule during the activation process. Therefore, the as-prepared **1** possesses high thermal stability and chemical stability and is completely insoluble in organic solvents.

3.3. FT-IR Spectra. Further verification of **1** for its chemical integrity was analyzed by FT-IR (Figure S8). Compound **1** exhibits a broad band in the region of 3101–3716 cm⁻¹, which may be ascribed to O–H and N–H stretching vibrations. The

typical $\nu(\text{C}=\text{O})$ stretching mode in the 1652–1767 cm^{-1} range indicates the presence of carbonyl or uncoordinated carboxylate groups in **1**. The peaks appearing at 1582 and 1622 cm^{-1} for antisymmetric stretching vibrations and a peak appearing at 1385 cm^{-1} for the symmetric stretching vibrations of **1** account for the presence of deprotonated carboxylate groups coordinated to the In^{3+} cations.³⁴ The peak observed at 1007–1105 cm^{-1} corresponds to the C–N stretching vibration, which further supports the formation of a new ligand **L**, in accordance with the results of X-ray diffraction analysis. Similar FT-IR peaks in the previous report also verified the chemical environments of **1**.³⁵

3.4. Gas Adsorption. The gas adsorption properties of **1** were investigated by N_2 adsorption analyses at 77 K and CO_2 adsorption analyses at 298 and 273 K. As shown in Figure 3,

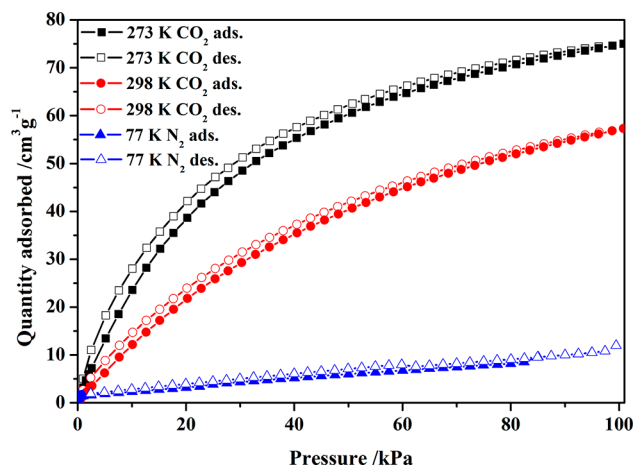


Figure 3. Comparison of the adsorption (solid symbols) and desorption (open symbols) isotherms of CO_2 at 273 and 298 K, as well as N_2 at 77 K, for **1**.

there is almost no N_2 adsorption at 77 K for **1**. However, **1** exhibits selective uptake for CO_2 . When the pressure P (actual pressure) approaches 101 kPa, the CO_2 uptake reaches 75.0 $\text{cm}^3 \text{g}^{-1}$ at 273 K and 57.3 $\text{cm}^3 \text{g}^{-1}$ at 298 K, respectively. The CO_2 adsorption isotherms reveal that the adsorption enthalpies (Q_{st}) of **1** at zero surface coverage is 20.8 kJ mol^{-1} using the Virial equation from sorption isotherms at 273 and 298 K (Figure S9),³⁶ which implies that **1** has a high binding ability to CO_2 . The observed value (20.8 kJ mol^{-1}) is higher than those of most “bench-mark MOFs”, such as MOF-5 (17 kJ mol^{-1})³⁷ and UMCM-1 (12 kJ mol^{-1}),³⁸ and is similar to that of CuBTTri (21 kJ mol^{-1}).³⁹ When the adsorption amount is converted to the numbers of CO_2 adsorbed in each molecule, it can be seen that ca. 2.4 CO_2 molecules per asymmetric unit of **1** are captured at 1 bar. The exposed open metal sites and protruded basic piperazine in the pore are proposed to play critical roles in the considerable CO_2 adsorption. Selective adsorption of CO_2 over N_2 is promising for application in CO_2/N_2 separation, which may be utilized in capturing greenhouse gas for environmental protection.

3.5. Lewis and Brønsted Acidity Characterization. In order to confirm the presence of Lewis and Brønsted acidic sites on **1**, we used in situ DRIFT spectroscopy for CO adsorption at 173 K. CO is an IR probe molecule for exploring the distribution of the Lewis and Brønsted acidic sites in a catalyst. As a dipole molecule, CO could form a σ bond with the cation through the C side with the cations, which indicates

information on the acidic sites of the catalyst.^{40a} Activated **1** of CO adsorption was measured as the background. As shown in Figure 4a, there were two small positive peaks at 2166 and 2131

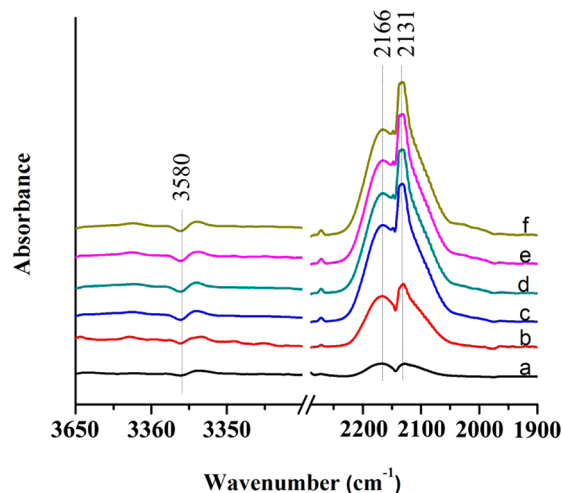


Figure 4. DRIFT spectra of CO adsorption on **1** at 173 K with increasing CO coverage.

cm^{-1} in the $\nu(\text{CO})$ vibrational region, which were caused by physisorption of CO on the surface of the material. Then we continued to increase the dosage of CO, tracking the changes of the adsorption. When the CO dosage increased, the peak at 2131 cm^{-1} significantly enhanced (Figure 4b–f), indicating that the material has positively charged Lewis acidic sites involved in **1**.^{40b} This is attributed to CO coordinated at open In^{3+} Lewis acidic sites, resulting in chemical adsorption. Meanwhile, the negative peak at 3580 cm^{-1} increasing with the amount of CO increased, which could be attributed to the decrease of the coordination strength between the hydroxyl group and In^{3+} , caused by the coordination of CO and In^{3+} . Hence, this peak originated from the MOF’s Brønsted acidic sites.^{40c} In brief, the DRIFT spectra of CO demonstrate that there are both Lewis and Brønsted acidic sites on **1**, which will benefit the CO_2 epoxidation reaction.

3.6. Catalytic Cycloaddition of CO_2 and Epoxides. On the basis of the high density of Lewis and Brønsted acidic sites on **1** and its capability of highly selective sorption of CO_2 at room temperature, we decided to evaluate **1** as a Lewis/Brønsted acidic bifunctional catalyst to catalyst cycloaddition of CO_2 and epoxides to form cyclic carbonates. During our investigation of various recent reports, we chose relatively mild conditions (Scheme 2, 2 MPa and 80 °C) in the presence of TBAB as the cocatalyst to study the catalytic ability of **1**, and the results are summarized in Table 1. It can be seen that the yield for PC for the reaction was very low when the catalyst or TBAB was absent in the system, under the employed reaction conditions (Table 1, entries 2 and 3), while the test on the combination of **1** and TBAB as a binary catalyst proved that it

Scheme 2. Cycloaddition of CO_2 with Different Epoxides

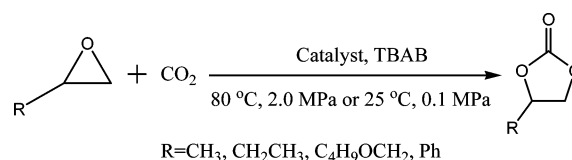
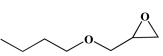
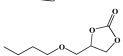


Table 1. Cycloaddition of CO₂ and Epoxide Using Different Catalysts under Various Reaction Conditions^a

Entry	Catalyst	Epoxides	Products	Catalyst (μmol)	Yield ^b (%)	TOF ^c (h^{-1})
1	None			-	0	0
2	1			46	8.9	9.7
3	TBAB			-	11.7	-
4	InCl ₃ /TBAB			27	91.9	170.2
5	1 /TBAB			26	57.2	110.0
6	1 /TBAB			36	75.7	105.1
7	1 /TBAB			46	93.9	102.1
8	1 /TBAB			56	93.4	83.4
9	1 /TBAB			46	90.7	98.6
10	1 /TBAB			46	85.3	92.7
11	1 /TBAB			46	73.2	79.7
12	InCl ₃ /TBAB			27	91.5	169.4

^aReaction conditions: epoxide, 20 mmol; TBAB, 0.5 mmol; CO₂ pressure, 2 MPa; reaction temperature, 80 °C; reaction time, 4 h. ^bYields were determined by GC. ^cMoles of yielded cyclic carbonate per mole of catalyst per hour.

can serve as an excellent catalyst for the synthesis of PC with a yield of 93.9% over 4 h [turnover frequency (TOF) 102.1 h⁻¹; Table 1, entry 7]. Thus, both **1** and TBAB perform a critical role and are indispensable in the reaction. It is proposed that TBAB was employed as a cocatalyst in all of the experiments, based on the previous reports.^{24,26,41} Interestingly, the activity of **1**/TBAB was similar to that of InCl₃/TBAB, in which InCl₃ is a widely used Lewis acidic homogeneous catalyst. A 91.9% yield (TOF 170.2 h⁻¹; Table 1, entry 4) of PC was achieved by the In³⁺-based catalyst (the amount of In cation is equal to the content of In in 46 μmol of **1**), which further underlines the potential application of **1** toward the CO₂ conversion reaction. At the same time, as shown in entries 5–8, 57.2%, 75.7%, 93.9%, and 93.4% yields of PC can be achieved when catalyst **1** with amounts from 26 to 56 μmol were employed. Therefore, it can be concluded that the amount of the catalyst has an important influence on the yield of PC. In other words, the concentration of the catalytic site determines the catalytic efficiency. A total of 46 μmol of catalyst afforded a satisfied yield of PC, so this catalyst loading amount was fixed for the following experiments. In addition, CO₂ cycloaddition with epoxides substituted with different functional groups has also been tested over **1**. With an increase of the molecular sizes of epoxide substrates, the yield of formation of cyclic carbonates just slightly decreased. The yields of butylene carbonate, 3-butoxy-1,2-propylene carbonate, and styrene carbonate were 90.7%, 85.3%, and 73.2%, respectively (Table 1, entries 9–11). This could be ascribed to the hindrance effect of the pores in **1** for different epoxides and corresponding products with large sizes, which slows the diffusion of the reactant and results in a decrease of the yield. A control experiment was carried out

using InCl₃/TBAB as the homogeneous catalyst for conversion of styrene oxide, while a 91.5% yield (TOF 169.4 h⁻¹; Table 1, entry 12) of styrene carbonate was achieved under the same conditions. This can further evidence that the reactions took place inside the pores and the hindrance effect of the pores affected the reaction directly.

The reaction was also carried out with **1** as catalyst at 1 atm CO₂ atmosphere and room temperature. As shown in Table 2, for the PC with a smaller size, a yield of 77.9% (TOF: 7.1 h⁻¹) is obtained (entry 1). The yields of butylene carbonate, 3-butoxy-1,2-propylene carbonate, and styrene carbonate reach to 60.1%, 44.2% and 31.6%, respectively, after 48 h (entries 2–4).

Table 2. Cycloaddition of CO₂ and Epoxides Using Catalyst **1** at 1 atm of CO₂ and Room Temperature^a

Entry	Epoxides	Products	Yield ^b (%)	TOF ^c (h^{-1})
1			77.9	7.1
2			60.1	5.4
3			44.2	4.0
4			31.6	2.9

^aReaction conditions: epoxide, 20 mmol; TBAB, 1 mmol; **1**, 46 μmol ; 1 atm of CO₂; room temperature; reaction time, 48 h. ^bYields were determined by GC. ^cMoles of yielded cyclic carbonate per mole of catalyst per hour.

The results indicated **1** not only can catalyze the CO₂ conversion reaction under high pressure and heated conditions efficiently, but also exhibit high activity under mild conditions, which could be due to the high CO₂ uptake ability and the high density of Lewis acid and Brønsted acid sites in **1**. To the best of our knowledge, only two Cu-MOFs^{26,42} and USTC-253²⁷ have been developed to accomplish such CO₂ cycloaddition conversion under similar mild conditions thus far.

The stability and recyclability of the catalyst are very important for heterogeneous catalysis. The recycling experiments were carried out after the catalyst recovered from the cycloaddition reaction by thorough a washing and drying process. Compared to the freshly prepared **1**, its PXRD pattern after catalysis showed no change in the peak intensity and position, which indicated the stability of **1** (Figure S10). Moreover, the IR spectra of **1** also confirmed that the structural integrity of **1** was well maintained after the catalytic experiments (Figure S8). A new peak appeared at around 1788 cm⁻¹, which was ascribed to the new generation of the carbonyl group in cyclic carbonate.⁴³ Thanks to its high thermal and chemical stability, the recovered **1** could maintain the integrity of the structure after catalysis. The catalytic activity of **1** still remained equal to the level of that of the freshly prepared during five cycles of recyclability tests for the cycloaddition of CO₂ and propylene oxide (PO; Figure 5).

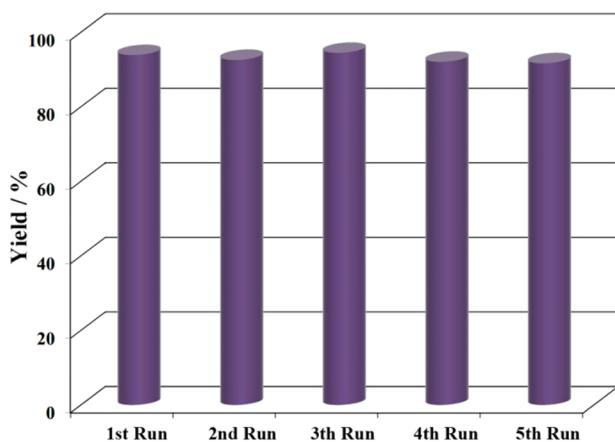
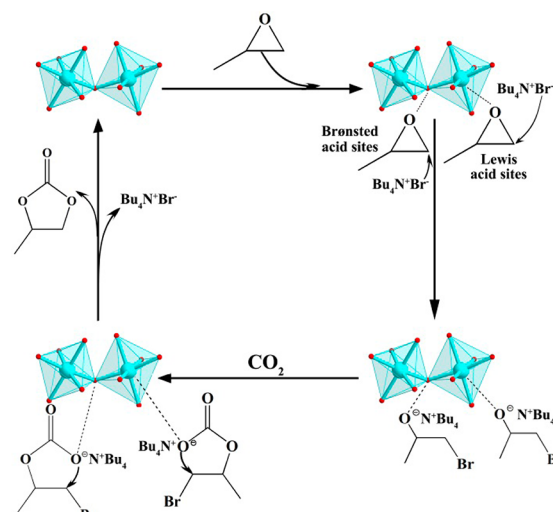


Figure 5. Recycle experiments of **1** for the cycloaddition of CO₂ and PO.

On the basis of the aforementioned experiments and previous reports,⁴⁴ the mechanism for the catalytic cycloaddition of epoxide and CO₂ into cyclic carbonate can be proposed to be the Lewis and Brønsted acidic based catalysis tentatively. As illustrated in Scheme 3, first, the O atom of epoxide molecules coordinates to the Lewis acidic centers (In³⁺ for **1**) or the Brønsted acidic sites, leading to activation of the epoxy ring; second, the Br⁻ from the TBAB acting as a nucleophile attacks the less-hindrance C of the epoxide, causing opening of the epoxy ring; third, an alkylcarbonate anion is formed by the interaction of CO₂ with the opened epoxy ring; fourth, for the final ring-closing step, the alkylcarbonate anion is cyclized to give the product of cyclic carbonate and, simultaneously, TBAB and catalyst are regenerated. It could be deduced that the synergistic effect of the high density of the Lewis and Brønsted acidic sites and the high uptake of CO₂ and TBAB in the confined pores of **1** promotes the cycloaddition

Scheme 3. Proposed Catalytic Mechanism for the Cycloaddition of CO₂ and PO Catalyzed by **1**



reaction, which thereby leads to high catalytic activity of **1** for chemical conversion of CO₂ into cyclic carbonates.

4. CONCLUSIONS

In conclusion, an In-based MOF with mixed linkers was constructed, in which part of 1,2,4-H₃btc was reacted with piperazine to generate a new ligand L. The in situ grafted piperazine not only helped to stabilize the framework but also benefited the CO₂ selective adsorption. The open metal sites act as Lewis acidic centers, and the μ₂-OH groups act as the Brønsted acidic centers, which were confirmed by DRIFT spectroscopy of CO adsorption on **1**. Compound **1** exhibited excellent performance as a Lewis/Brønsted acidic bifunctional heterogeneous catalyst for chemical fixation of CO₂ coupling with epoxides into cyclic carbonates under mild conditions. Significantly, the catalyst possesses superb recyclability, and its activity showed no decrease during five cycles of reaction. The strategy for the fabrication of stable MOFs reported in this work would open a new door for the integration of CO₂ capture and conversion. Research along this line is going on in our laboratory.

■ ASSOCIATED CONTENT

Supporting Information

The Supporting Information is available free of charge on the ACS Publications website at DOI: 10.1021/acs.inorgchem.6b00050.

Crystal structures, ¹³C CPMAS NMR and ¹H NMR spectra of **1** and 1,2,4-H₃btc, TG curves of **1**, PXRD pattern of **1**, FT-IR spectra, isosteric adsorption enthalpy of CO₂ on **1**, and X-ray crystallographic data for **1** (PDF) X-ray crystallographic data for **1** in CIF format (CIF)

■ AUTHOR INFORMATION

Corresponding Authors

*E-mail: ceshzb@lnu.edu.cn (Z.-B.H.).

*E-mail: jianglab@ustc.edu.cn (H.-L.J.).

Author Contributions

The manuscript was written through contributions of all authors. All authors have given approval to the final version of the manuscript.

Notes

The authors declare no competing financial interest.

ACKNOWLEDGMENTS

This work was granted financial support from the National Natural Science Foundation of China (Grants 20871063, 21271096, 21501084, 21371162, 51301159, and 21521001), the 973 program (Grant 2014CB931803), the Research Fund for the Doctoral Program of Higher Education of China (Grant 20133402120020), the Recruitment Program of Global Youth Experts, and the Fundamental Research Funds for the Central Universities (Grant WK2060190026). We gratefully thank Mr. Hengwei Wang and Prof. Junling Lu at USTC for kind help in the CO-IR experiment.

REFERENCES

- (1) Allen, M. R.; Frame, D. J.; Huntingford, C.; Jones, C. D.; Lowe, J. A.; Meinshausen, M.; Meinshausen, N. *Nature* **2009**, *458*, 1163–1166.
- (2) (a) Quadrelli, R.; Peterson, S. *Energy Policy* **2007**, *35*, 5938–5952. (b) Xiang, S.; He, Y.; Zhang, Z.; Wu, H.; Zhou, W.; Krishna, R.; Chen, B. *Nat. Commun.* **2012**, *3*, 954–963. (c) Lee, W. R.; Hwang, S. Y.; Ryu, D. W.; Lim, K. S.; Han, S. S.; Moon, D.; Choi, J.; Hong, C. S. *Energy Environ. Sci.* **2014**, *7*, 744–751.
- (3) (a) Klein, R. J. T.; Schipper, E. L. F.; Dessai, S. *Environ. Sci. Policy* **2005**, *8*, 579–588. (b) Najam, A.; Rahman, A. A.; Huq, S.; Sokona, Y. *Climate Policy* **2003**, *3*, S9–S17. (c) Peters, G. P.; Hertwich, E. G. *Environ. Sci. Technol.* **2008**, *42*, 1401–1407.
- (4) (a) Li, J.-R.; Ma, Y.; McCarthy, M. C.; Sculley, J.; Yu, J.; Jeong, H.-K.; Balbuena, P. B.; Zhou, H.-C. *Coord. Chem. Rev.* **2011**, *255*, 1791–1823. (b) Álvaro, A. J.; Paniagua, I. L.; Fernández, C. G.; Martín, J. R.; Carlier, R. N. *Energy Convers. Manage.* **2015**, *104*, 170–179. (c) Boot-Handford, M. E.; Abanades, J. C.; Anthony, E. J.; Blunt, M. J.; Brandani, S.; MacDowell, N.; Fernández, J. R.; Ferrari, M.-C.; Gross, R.; Hallett, J. P.; Haszeldine, R. S.; Heptonstall, P.; Lyngfelt, A.; Makuch, Z.; Mangano, E.; Porter, R. T. J.; Pourkashanian, M.; Rochelle, G. T.; Shah, N.; Yao, J. G.; Fennell, P. S. *Energy Environ. Sci.* **2014**, *7*, 130–189.
- (5) (a) Rochelle, G. T. *Science* **2009**, *325*, 1652–1654. (b) Liu, J.; Thallapally, P. K.; McGrail, B. P.; Brown, D. R.; Liu, J. *Chem. Soc. Rev.* **2012**, *41*, 2308–2322.
- (6) (a) Sakakura, T.; Choi, J.-C.; Yasuda, H. *Chem. Rev.* **2007**, *107*, 2365–2387. (b) Sakakura, T.; Saito, Y.; Okano, M.; Choi, J.-C.; Sako, T. *J. Org. Chem.* **1998**, *63*, 7095–7096. (c) Tian, J.-S.; Miao, C.-X.; Wang, J.-Q.; Cai, F.; Du, Y.; Zhao, Y.; He, L.-N. *Green Chem.* **2007**, *9*, 566–571. (d) Zhang, Z.; Xie, Y.; Li, W.; Hu, S.; Song, J.; Jiang, T.; Han, B. *Angew. Chem., Int. Ed.* **2008**, *47*, 1127–1129.
- (7) (a) Yoshida, M.; Ihara, M. *Chem. - Eur. J.* **2004**, *10*, 2886–2893. (b) Bayardon, J.; Holz, J.; Schäffner, B.; Andrushko, V.; Verevkin, S.; Preetz, A.; Börner, A. *Angew. Chem., Int. Ed.* **2007**, *46*, 5971–5974.
- (8) (a) Schäffner, B.; Schäffner, F.; Verevkin, S. P.; Börner, A. *Chem. Rev.* **2010**, *110*, 4554–4581. (b) Kim, H. S.; Kim, J. J.; Lee, B. G.; Jung, O. S.; Jang, H. G.; Kang, S. O. *Angew. Chem., Int. Ed.* **2000**, *39*, 4096–4098.
- (9) (a) Caló, V.; Nacci, A.; Monopoli, A.; Fanizzi, A. *Org. Lett.* **2002**, *4*, 2561–2563. (b) Wang, J.; Yang, J. G. W.; Yi, G.; Zhang, Y. *Chem. Commun.* **2015**, *51*, 15708–15711.
- (10) (a) Kawanami, H.; Sasaki, A.; Matsui, K.; Ikushima, Y. *Chem. Commun.* **2003**, 896–897. (b) Xu, B.-H.; Wang, J.-Q.; Sun, J.; Huang, Y.; Zhang, J.-P.; Zhang, X.-P.; Zhang, S.-J. *Green Chem.* **2015**, *17*, 108–122. (c) Kim, Y. J.; Varma, R. S. *J. Org. Chem.* **2005**, *70*, 7882–7891.
- (11) Jagtap, S. R.; Bhanushali, M. J.; Panda, A. G.; Bhanage, B. M. *Catal. Lett.* **2006**, *112*, 51–55.
- (12) (a) Iksi, S.; Aghmiz, A.; Rivas, R.; González, M. D.; Cuesta-Aluja, L.; Castilla, J.; Orejón, A.; El Guemmout, F. E.; Masdeu-Bultó, A. M. *J. Mol. Catal. A: Chem.* **2014**, *383–384*, 143–152. (b) Ulusoy, M.; Şahin, O.; Kilic, A.; Büyükgüngör, O. *Catal. Lett.* **2011**, *141*, 717–725.
- (13) (a) Decortes, A.; Belmonte, M. M.; Benet-Buchholz, J.; Kleij, A. W. *Chem. Commun.* **2010**, *46*, 4580–4582. (b) Tian, D.; Liu, B.; Gan, Q.; Li, H.; Darensbourg, D. J. *ACS Catal.* **2012**, *2*, 2029–2035.
- (14) Yamaguchi, K.; Ebitani, K.; Yoshida, T.; Yoshida, H.; Kaneda, K. *J. Am. Chem. Soc.* **1999**, *121*, 4526–4527.
- (15) (a) Xie, Y.; Zhang, Z.; Jiang, T.; He, J.; Han, B.; Wu, T.; Ding, K. *Angew. Chem., Int. Ed.* **2007**, *46*, 7255–7258. (b) Meng, X.-L.; Nie, Y.; Sun, J.; Cheng, W.-G.; Wang, J.-Q.; He, H.-Y.; Zhang, S.-J. *Green Chem.* **2014**, *16*, 2771–2778.
- (16) (a) Srivastava, R.; Srinivas, D.; Ratnasamy, P. *Appl. Catal., A* **2005**, *289*, 128–134. (b) Kinage, A. K.; Gupte, S. P.; Chaturvedi, R. K.; Chaudhari, R. V. *Catal. Commun.* **2008**, *9*, 1649–1655.
- (17) (a) Furukawa, H.; Muller, U.; Yaghi, O. M. *Angew. Chem., Int. Ed.* **2015**, *54*, 3417–3430. (b) Nugent, P.; Belmabkhout, Y.; Burd, S. D.; Cairns, A. J.; Luebke, R.; Forrest, K.; Pham, T.; Ma, S.; Space, B.; Wojtas, L.; Eddaoudi, M.; Zaworotko, M. J. *Nature* **2013**, *495*, 80–84.
- (18) (a) Sumida, K.; Rogow, D. L.; Mason, J. A.; McDonald, T. M.; Bloch, E. D.; Herm, Z. R.; Bae, T.-H.; Long, J. R. *Chem. Rev.* **2012**, *112*, 724–781. (b) Fracaroli, A. M.; Furukawa, H.; Suzuki, M.; Dodd, M.; Okajima, S.; Gándara, F.; Reimer, J. A.; Yaghi, O. M. *J. Am. Chem. Soc.* **2014**, *136*, 8863–8866. (c) Choi, S.; Drese, J. H.; Jones, C. W. *ChemSusChem* **2009**, *2*, 796–854.
- (19) (a) An, J.; Geib, S. J.; Rosi, N. L. *J. Am. Chem. Soc.* **2010**, *132*, 38–39. (b) Yuan, B.; Ma, D.; Wang, X.; Li, Z.; Li, Y.; Liu, H.; He, D. *Chem. Commun.* **2012**, *48*, 1135–1137. (c) Mu, Q.; Wang, H.; Li, L.; Wang, C.; Wang, Y.; Zhao, X. *Chem. - Asian J.* **2015**, *10*, 1864–1869. (d) Vaidhyanathan, R.; Iremonger, S. S.; Shimizu, G. K. H.; Boyd, P. G.; Alavi, S.; Woo, T. K. *Science* **2010**, *330*, 650–653.
- (20) (a) Lee, J.; Farha, O. K.; Roberts, J.; Scheidt, K. A.; Nguyen, S. T.; Hupp, J. T. *Chem. Soc. Rev.* **2009**, *38*, 1450–1459. (b) Ma, L. Q.; Abney, C.; Lin, W. B. *Chem. Soc. Rev.* **2009**, *38*, 1248–1256. (c) Liu, Y.; Howarth, A. J.; Hupp, J. T.; Farha, O. K. *Angew. Chem., Int. Ed.* **2015**, *54*, 9001–9005. (d) Dhakshinamoorthy, A.; Garcia, H. *Chem. Soc. Rev.* **2012**, *41*, 5262–5284.
- (21) Macias, E. E.; Ratnasamy, P.; Carreon, M. A. *Catal. Today* **2012**, *198*, 215–218.
- (22) Miralda, C. M.; Macias, E. E.; Zhu, M.; Ratnasamy, P.; Carreon, M. A. *ACS Catal.* **2012**, *2*, 180–183.
- (23) Zalomaeva, O. V.; Chibiryaev, A. M.; Kovalenko, K. A.; Kholdeeva, O. A.; Balzhinimaev, B. S.; Fedin, V. P. *J. Catal.* **2013**, *298*, 179–185.
- (24) Song, J.; Zhang, Z.; Hu, S.; Wu, T.; Jiang, T.; Han, B. *Green Chem.* **2009**, *11*, 1031–1036.
- (25) Kim, J.; Kim, S.-N.; Jang, H.-G.; Seo, G.; Ahn, W.-S. *Appl. Catal., A* **2013**, *453*, 175–180.
- (26) Gao, W. Y.; Chen, Y.; Niu, Y.; Williams, K.; Cash, L.; Perez, P. J.; Wojtas, L.; Cai, J.; Chen, Y. S.; Ma, S. *Angew. Chem., Int. Ed.* **2014**, *53*, 2615–2619.
- (27) Jiang, Z. R.; Wang, H.; Hu, Y.; Lu, J.; Jiang, H. L. *ChemSusChem* **2015**, *8*, 878–885.
- (28) Han, Z.-B.; Song, Y.-J.; Ji, J.-W.; Zhang, W.; Han, G.-X. *J. Solid State Chem.* **2009**, *182*, 3067–3070.
- (29) Sheldrick, G. M. *SHELXS-2014, Program for the solution and refinement of crystal structures*; University of Göttingen: Göttingen, Germany, 2014.
- (30) Koh, K.; Wong-Foy, A. G.; Matzger, A. J. *Angew. Chem., Int. Ed.* **2008**, *47*, 677–680.
- (31) Spek, A. L. *PLATON*; Utrecht University: Utrecht, The Netherlands, 1998.
- (32) Wang, J.-H.; Li, M.; Li, D. *Chem. - Eur. J.* **2014**, *20*, 12004–12008.
- (33) Furukawa, H.; Gándara, F.; Zhang, Y.-B.; Jiang, J.; Queen, W. L.; Hudson, M. R.; Yaghi, O. M. *J. Am. Chem. Soc.* **2014**, *136*, 4369–4381.

- (34) Liu, L.; Zhang, X.-N.; Han, Z.-B.; Gao, M.-L.; Cao, X.-M.; Wang, S.-M. *J. Mater. Chem. A* **2015**, *3*, 14157–14164.
- (35) Liu, W.; Yu, J.; Jiang, J.; Yuan, L.; Xu, B.; Liu, Q.; Qu, B.; Zhang, G.; Yan, C. *CrystEngComm* **2011**, *13*, 2764–2773.
- (36) Czepirski, L.; Jagiello, J. *Chem. Eng. Sci.* **1989**, *44*, 797–801.
- (37) Choi, J.-S.; Son, W.-J.; Kim, J.; Ahn, W.-S. *Microporous Mesoporous Mater.* **2008**, *116*, 727–731.
- (38) Mu, B.; Schoenecker, P. M.; Walton, K. S. *J. Phys. Chem. C* **2010**, *114*, 6464–6471.
- (39) Demessence, A. D.; D'Alessandro, D. M.; Foo, M. L.; Long, J. R. *J. Am. Chem. Soc.* **2009**, *131*, 8784–8786.
- (40) (a) Huber, S.; Knözinger, H. *Appl. Catal., A* **1999**, *181*, 239–244. (b) Zou, R.-Q.; Sakurai, H.; Han, S.; Zhong, R.-Q.; Xu, Q. *J. Am. Chem. Soc.* **2007**, *129*, 8402–8403. (c) Ravon, U.; Chaplais, G.; Chizallet, C.; Seyyedi, B.; Bonino, F.; Bordiga, S.; Bats, N.; Farrusseng, D. *ChemCatChem* **2010**, *2*, 1235–1238.
- (41) Beyzavi, M. H.; Stephenson, C. J.; Liu, Y.; Karagiari, O.; Hupp, J. T.; Farha, O. K. *Front. Energy Res.* **2015**, *2*, 63.
- (42) Gao, W.-Y.; Wojtas, L.; Ma, S. *Chem. Commun.* **2014**, *50*, 5316–5318.
- (43) Chen, C.; Zhang, J.; Li, G.; Shen, P.; Jin, H.; Zhang, N. *Dalton Trans.* **2014**, *43*, 13965–13971.
- (44) Zhu, M.; Carreon, M. A. *J. Appl. Polym. Sci.* **2014**, *131*, 39738.